ROYAL SOCIETY
OF CHEMISTRY

PAPER

Check for updates

Slice imaging study of NO$_2$ photodissociation *via* the 1^{2}B$_2$ and 2^{2}B$_2$ states: the NO(X$^2\Pi$) + O(^{3}P$_J$) product channel†

Zhaoxue Zhang, [ab] Shuaikang Yang, [b] Zhenxing Li,*[b] Yao Chang, [b] Zijie Luo, [b] Yarui Zhao, [b] Shengrui Yu, *[a] Kaijun Yuan *[bc] and Xueming Yang [bcd]

The state-resolved photodissociation of NO$_2$ *via* the 1^{2}B$_2$ and 2^{2}B$_2$ excited states has been investigated by using time-sliced velocity-mapped ion imaging technique. The images of the O(^{3}P$_{J=2,1,0}$) products at a series of excitation wavelengths are measured by employing a 1 + 1′ photoionization scheme. The total kinetic energy release (TKER) spectra, NO vibrational state distributions and anisotropy parameters (β) are derived from the O(^{3}P$_{J=2,1,0}$) images. For the 1^{2}B$_2$ state photodissociation of NO$_2$, the TKER spectra mainly present a non-statistical vibrational state distribution of the NO co-products, and the profiles of most vibrational peaks display a bimodal structure. The β values show a gradual decrease with the photolysis wavelength increasing except for a sudden increase at 357.38 nm. The results suggest that the NO$_2$ photodissociation *via* the 1^{2}B$_2$ state proceeds *via* the non-adiabatic transition between the 1^{2}B$_2$ and X̃^{2}A$_1$ states, leading to the NO(X$^2\Pi$) + O(^{3}P$_J$) products with wavelength-dependent rovibrational distributions. As for photodissociation of NO$_2$ *via* the 2^{2}B$_2$ state, the NO vibrational state distribution is relatively narrow with the main peak shifting from v = 1, 2 at 235.43–249.22 nm to v = 6 at 212.56 nm. The β values exhibit two distinctly different angular distributions, *i.e.*, near isotropic at 249.22 and 246.09 nm and anisotropic at the rest of the excitation wavelengths. These results are consistent with the fact that the 2^{2}B$_2$ state potential energy surface has a barrier, and the dissociation process is fast when the initial populated level is above this barrier. A bimodal vibrational state distribution is clearly observed at 212.56 nm, in which the main distribution (peaking at v = 6) is ascribed to dissociation *via* an avoided crossing with the higher electronically excited state while the subsidiary distribution (peaking at v = 11) likely arises due to dissociation *via* the internal conversion to the 1$_2$B$_2$ state or to the X̃ ground state.

I. Introduction

Nitrogen dioxide (NO$_2$) has 17 valence electrons that result in a bent geometry with an equilibrium bond angle of $\sim$134.25°. When the low-lying adiabatic potentials are excited, this open-shell electronic structure would lead to highly coupled electronic states and complicated non-adiabatic decomposition dynamics.[1,2]

^{a} *Hangzhou Institute of Advanced Studies, Zhejiang Normal University, 1108 Gengwen Road, Hangzhou, Zhejiang 311231, P. R. China. E-mail: sryu@zjnu.cn*

^{b} *State Key Laboratory of Molecular Reaction Dynamics and Dalian Coherent Light Source, Dalian Institute of Chemical Physics, Chinese Academy of Sciences, 457 Zhongshan Road, Dalian, Liaoning 116023, P. R. China. E-mail: lzx2015@dicp.ac.cn, kjyuan@dicp.ac.cn*

^{c} *Hefei National Laboratory, Hefei 230088, China*

^{d} *Department of Chemistry and Center for Advanced Light Source Research, College of Science, Southern University of Science and Technology, Shenzhen 518055, China*

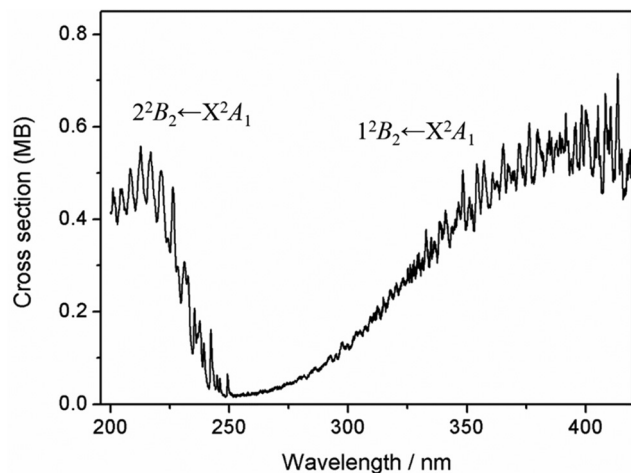† Electronic supplementary information (ESI) available. See DOI: https://doi.org/10.1039/d3cp00420a

Furthermore, as a primary precursor for the formation of photochemical smog, NO$_2$ is strongly involved in the formation and destruction process of ozone.[3] It is also suggested that the reaction of the electronically excited NO$_2$ molecules with water might be an additional source of OH radicals in the earth's troposphere.[4] Therefore, great efforts have been made to investigate state-resolved photodissociation dynamics of NO$_2$ over the past sixty years.

The NO$_2$ absorption spectrum displays two broad and structured features in the ultraviolet (UV)-visible region, as shown in Fig. 1.[1,5–7] The first absorption band of NO$_2$ extends from 667 to 250 nm with a peak near 400 nm. This band is associated with the excitation from the X̃^{2}A$_1$ ground state to the 1^{2}B$_1$ and 1^{2}B$_2$ excited electronic states with the majority of the oscillator strength lying on the 1^{2}B$_2$ ← X̃^{2}A$_1$ transition.[8] The vibronic coupling of the excited 1^{2}B$_2$ state to the other energetically accessible electronic states, like 1^{2}B$_1$ and 1^{2}A$_2$ states, further complicates the absorption spectrum.[9] A rapid non-adiabatic transition through a conical intersection between the

Fig. 1 The UV absorption spectrum of NO_2 between 200 and 450 nm ($1MB = 1 \times 10^{-18}$ cm^2 mol^{-1}). The main transitions of the absorption bands have been marked in the figure.

1^2B_2 and $\tilde{X}$ states transfers the excited state population back to the ground state, where decay into products occurs. The first spin-allowed dissociation channel of NO_2 is as follows:

$$NO_2 + h\nu \rightarrow NO(X^2\Pi) + O(^3P_2), \quad \lambda \leq 398.0 \text{ nm}$$
(1)
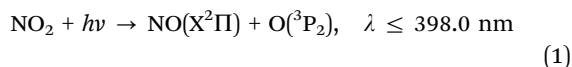
The thermodynamical threshold of this channel has been determined by Jost and coworkers.[10] Since then, numerous photodissociation studies of NO_2 in the first absorption band have been carried out.[11–24] In the 1990s, the experiments were mainly performed at a single photolysis wavelength of 355 nm.[11–17] In these studies, the angular distribution for $O(^3P_2)$ at 355 nm was described by the anisotropy parameter of $\beta = 1.2 \pm 0.3$,[16] and the lifetime of $NO_2(1^2B_2)$ state was estimated to be ~ 250 fs.[18] Harrison et al.[14] determined the vibrational state population of NO (ν = 0, 1) in the photodissociation of NO_2 at 355 and 351 nm by using the photofragment translational spectroscopy. The results were consistent with the trend predicted by statistical models of the dissociation process. However, the observed bimodal rotational distributions of NO (ν = 0, 1) also indicated non-statistical decay dynamics. Recently, the velocity-mapped ion imaging method has been applied to the photodissociation of NO_2 at 308 nm by detection of the $O(^3P_J)$ atomic products.[11] The non-statistical NO vibrational state distribution was pointed to a dynamical dissociation mechanism. Further studies on the product distributions suggested that at low excess energies, the unimolecular decay can be described, at least on average, using statistical theories. But, at higher excess energies, where the dissociation becomes more rapid, such models cease to be valid.[20–24]

Compared to the first absorption band, the second absorption band starting from ~ 250 nm shows a much simpler vibrational structure, which has a broad maximum at ~ 217 nm.[6] Theoretical calculations[4] clearly verified that this UV band is due to excitation of the 2^2B_2 state (commonly termed the $\tilde{D}^2B_2$ state). Detailed rotational analysis of $\tilde{D}(000)$ band has been carried out and the

lifetime of $\sim 42 \pm 5$ ps has been extracted by Hallin and Merer.[25] The lifetime rapidly decreased to sub-100 fs with decreasing wavelength from 250 nm to 235 nm, and a series of discrete vibronic absorption bands in this range have been clearly assigned.[4,26,27] While the diffuse structures below 230 nm showed a progression with an average spacing of 940 cm^{-1}, which were attributed to symmetric stretching vibrational excitation of the 2^2B_2 state.[4] In this absorption band, the $O(^1D)$ production becomes energetically allowed and is produced with a near constant quantum yield of around 50% between 244 and 193 nm.[28–30]

It is believed that single-photon dissociation of NO_2 via the 2^2B_2 state produced NO with low rotational, but high vibrational excitation.[31,32] The photolysis of NO_2 at 248 nm resulted in a very sharply peaked vibrational distribution of NO(ν) from channel (1) has been previously observed.[31,33,34] Slanger et al.[31] reported that the NO vibrational state population peaking at ν = 7, close to the maximum energetically possible NO(ν) level at 248 nm photolysis. In contrast, Wilkinson and Whitaker[35] argued that the $NO(X^2\Pi) + O(^3P_J)$ channel at 226 nm favored the production of vibrationally cold, but high rotationally excited NO products. At an even shorter excitation wavelength, Ahmed et al.[36] reported a bimodal translational energy distribution for the $O(^3P_J)$ channel at 212.8 nm, with a major peak corresponding to $NO(X^2\Pi, \nu = 4)$ and a minor peak ascribing to $NO(X^2\Pi, \nu = 10–11)$. Coroiu et al.[37] also found that the kinetic energy of the $O(^3P_J)$ fragments was consistent with production in coincidence with $NO(X^2\Pi)$ in ν = 7 and ν = 13–14 in the ~ 200 nm photodissociation of NO_2. It was suggested that NO_2 with more or less bending and symmetric stretching excitation will dissociate via at least two adiabatic surfaces, which leads to such bimodal energy distribution.[11,35–38]

To date, photodissociation of NO_2 has been studied extensively in the first and second UV absorption bands, but it still paints a confusing and often contradictory picture of the dissociation mechanism. Furthermore, the NO vibrational state population distributions are not consistent in previous studies. In this work, we provide the state-resolved photodissociation study of NO_2 at a series of excitation wavelengths, which span two main UV absorption bands. The TKER spectra and anisotropy parameters β derived from the $O(^3P_{J=2,1,0})$ images exhibit a wavelength-dependent non-adiabatic dissociation dynamical picture of NO_2 via the 1^2B_2 and 2^2B_2 states. This study offers a whole and reliable dissociation feature of NO_2 and is beneficial to further understanding of the non-adiabatic interactions in the dissociation dynamics of polyatomic molecules.

II. Experimental method

The experiment apparatus used in this study has been described in previous publications.[39–42] Briefly, the pulsed supersonic molecular beam was generated by expanding a mixture of 10% NO_2 and He into the source chamber via a pulsed valve (General valve, Parker Series 9), where it was skimmed before entering and propagating along the centre axis of the ion optics assembly

This journal is © the Owner Societies 2023

Phys. Chem. Chem. Phys., 2023, **25**, 16872–16880 | **16873**

(IOA, 23-plate ion optics) mounted in the reaction chamber. The molecular beam was intersected at right angles by the photolysis and probe laser beams between the second and third plates of the ion optics assembly. Noted that the valve was held at 383 K in order to push the NO_2/N_2O_4 equilibrium to 99.9% in favor of the monomer.[35] Thus, the signal from N_2O_4 photodissociation in this work is negligible. The NO_2 molecules were photodissociated by absorbing one photon of 212–250 and 300–365 nm. The nascent $O(^3P_J)$ products from NO_2 photodissociation were state-selectively ionized by using $1 + 1'$ (~ 130 nm + ~ 600 nm) photoionization scheme via the $^3S°$ [$2S^22P^3(4S°)3S$] intermediate state. Previous studies usually applied $(2 + 1)$ resonance enhancing multiphoton ionization (REMPI) at ~ 226 nm to ionize the oxygen atom.[11,36] This may cause multiphoton dissociation processes, for instance, the combination of photolysis laser and the 226 nm laser could lead to further generation of oxygen products, while $1 + 1'$ photoionization scheme significantly suppressed these processes. The resulting O^+ ions were then accelerated by the ion optics and passed through a 740 mm long time-of-flight tube before hitting a position-sensitive dual microchannel plate (MCP) coupled to a P43 phosphor screen. Transient images on the phosphor screen were recorded using a charge-coupled device (CCD) camera (Imager pro plus 2M, La Vision), using a 20 ns gate pulse voltage (which slices $\sim 10\%$ of the total Newton sphere distribution of the ions) in order to acquire time sliced images.

The laser system consisted of two Nd:YAG lasers and four dye lasers. The laser beam in the UV region generated by frequency doubling the output of the Nd:YAG I (Beamtech, SGR-20) laser pumped dye laser I (Corbra-Stretch, Sirah) was used to photolysis the NO_2 molecules. The Nd:YAG II (Continuum, Powerlite 9030) and other three dye lasers (Corbra-Stretch, Sirah) were designed to generate the $1 + 1'$ detection laser beams for ionizing $O(^3P_J)$ atomic products. The VUV light beam (130.172 nm for $O(^3P_2)$, 130.44 nm for $O(^3P_1)$, and 130.576 nm for $O(^3P_0)$) was generated by the four-wave mixing ($\omega_{VUV} = 2\omega_1 - \omega_2$) process. The laser light at 212.55 nm (ω_1) was generated by doubling the fundamental output of the dye laser II, which was pumped by the 355 nm laser light generated by the Nd:YAG II. The second harmonic output (532 nm) of the Nd:YAG II laser was split into two parts to separately pump the dye laser III and IV, respectively. The fundamental output of the dye laser III used as ω_2 (~ 570 nm) was Doppler scanned to measure O atomic products with different velocities. ω_1 and ω_2 were spatially and temporally overlapped and focused into a stainless-steel mixing cell filled with ~ 15 torr Krypton gas. The fundamental frequency output from the dye laser IV was employed as the second visible detection laser beam (~ 600 nm).

III. Results and discussion

A. Photodissociation of NO_2 via the 1^2B_2 state

Fig. 1 shows the UV absorption spectrum of the NO_2 molecules between 200 and 450 nm. The diffuse vibrational progressions are indicative of the mixed character of the excited potential energy surfaces (PESs). This complicated behavior is mainly ascribed to the strong mixing of the initial populated 1^2B_2 state with the X̃ ground state due to a low-lying conical intersection between these two PESs.[9] The Renner–Teller interaction[3] between the 1^2B_1 excited state and the X̃ ground state is also responsible for it. Besides, the spin–orbit interactions of all three states with the 1^2A_2 excited state further increase the complexity. Hence, the photodissociation of NO_2 in this spectrum region would be interesting and fascinating. Fig. 2 shows the images of $O(^3P_2)$ products and the corresponding total kinetic energy release (TKER) spectra at (a) 300.02 nm, (b) 310.05 nm, (c) 320.12 nm, (d) 348.38 nm, (e) 357.13 nm, and (f) 365.38 nm, respectively. The double-headed red arrow indicates the polarization direction of the dissociation lasers. Clearly, the partially resolved concentric ring structures in each image correspond to the different rovibrational states of the $NO(X^2\Pi)$ co-products. Besides the $O(^3P_2)$ products, the images of $O(^3P_1)$ and $O(^3P_0)$ products at these six photolysis wavelengths have also been detected (shown in Fig. S1 and S2, ESI†). By comparing the $O(^3P_{J=1,0})$ images and the TKER spectra to those in Fig. 2, they exhibit similar dynamics for the three $O(^3P_{J=2,1,0})$ spin–orbit dissociation channels.

According to the conservation of momentum and energy, the TKER spectra of the NO + O products can be expressed by the following equation:

$$TKER = E_{KE}(NO) + E_{KE}(O) = E_{KE}(O)(1 + m_O/m_{NO}),$$

$$= h\nu - D_0(NO–O) - E_{int}(NO) - E_{int}(O), \qquad (2)$$

where $E_{KE}(NO)$ and $E_{KE}(O)$ represent the kinetic energy of NO and O products (the $E_{KE}(O)$ can be directly derived from the $O(^3P_J)$ images), m_O and m_{NO} are the relative atomic mass of NO and O products, $h\nu$ is the photon energy, $D_0(NO–O)$ is the dissociation energy, $E_{int}(NO)$ is the internal energy distributions of NO products, and $E_{int}(O)$ is the energy of the $^3P_{J=1,0}$ state defined relative to the $^3P_2$ ground state of O atom. All of the TKER spectra in Fig. 2 display a series of partially resolved peaks extending to the available energy limit. As marked on the upper part of the TKER spectra, the partially-resolved peaks can be assigned to the $NO(X^2\Pi, \nu)$ vibrational states. Noted that the spin–orbit splitting of the $NO(X^2\Pi_{1/2,3/2})$ state is 119.82 cm^{-1}, which is not observed in this study due to the limited experimental resolution.[37] The TKER spectra in Fig. 2(a)–(f) show a non-statistical vibrational distribution, which is similar to previous studies on the photodissociation of the triatomic molecules, such as CO_2,[40] OCS,[43] and CS_2.[44] Furthermore, most of the vibrational peaks in Fig. 2 display a bimodal rotational structure. Such anomalous rotational population of NO products is similar to that observed in the NO_2 photodissociation study by Slanger et al.[31] and Zacharias et al.,[21] but different from that observed by Elofson et al.,[19] in which a statistical rotational distribution was observed. Previous studies reported that excitation around 337 nm involves both the 1^2B_2 and 1^2B_1 excited states, and these two states have respective equilibrium angles of 111°[45] and 180°,[46] substantially different from 134.25° of the X̃ ground state. The high rotational excitation

16874 | *Phys. Chem. Chem. Phys.*, 2023, **25**, 16872–16880

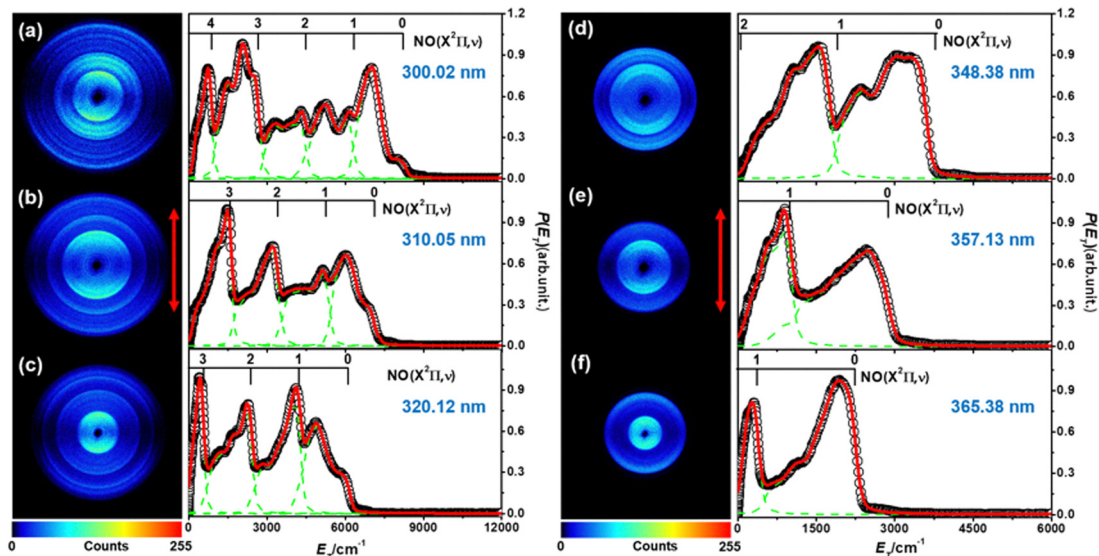This journal is © the Owner Societies 2023

Fig. 2 The images and TKER spectra of $O(^3P_2)$ products from NO_2 photodissociation at the wavelengths of (a) 300.02 nm, (b) 310.05 nm, (c) 320.12 nm, (d) 348.38 nm, (e) 357.13 nm and (f) 365.38 nm. The double headed red arrow indicates the polarization direction of the photolysis laser beam. The rings shown in the images correspond to the vibrational state of the $NO(^2\Pi)$ co-products. The open circles represent the experimental data and the red solid curves display the best fitting of the experimental spectra. The dashed green curves represent the simulated NO vibrational profile.

of NO can thus result from the decay of NO_2 in highly excited bending vibrational states.

To abstract more information, a qualitative simulation of the TKER spectra is carried out. In the fitting, a Gaussian-like shape is used to simulate the population of each rotational state. The intensities of each NO rotational state are then adjusted to produce a summed simulated TKER spectrum that best matches the experimental data. This process is complicated by the overlap of rotational levels associated with different vibrational states of the NO product, which can obscure the
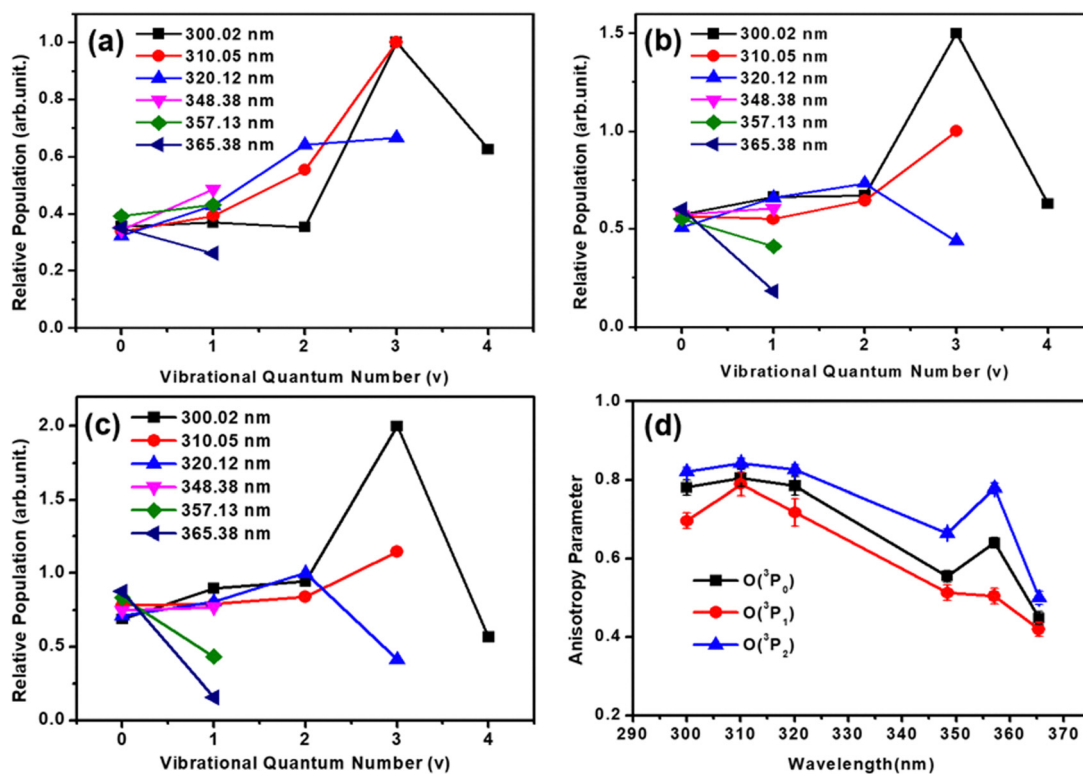

Fig. 3 (a–c) Relative vibrational state population of the NO co-products from NO + $O(^3P_{J=2,1,0})$ channels at six different photolysis wavelengths between 365 and 300 nm. (d) The anisotropy parameter β values derived from simulations of the images for $O(^3P_{J=2,1,0})$ products.

This journal is © the Owner Societies 2023

Phys. Chem. Chem. Phys., 2023, **25**, 16872–16880 | **16875**

relative contributions of the different levels in the simulation, but is helped by the expectation that the rotational population distributions associated with each vibrational state should vary relatively smoothly with the rotational quantum number. The relative vibrational state population distribution of NO products corresponding to the three $O(^3P_{J=2,1,0})$ product channels are acquired and depicted in Fig. 3(a)–(c). Apparently, the vibrational state populations of NO products at 300.02, 310.05, 320.12 and 348.38 nm are all inverted with a maximum in $\nu = 2$ or $\nu = 3$. These point to a dynamical, rather than a statistical dissociation mechanism at these wavelengths. A tentative conclusion drawn by George et al.[47] is that the vibrational excitations of nascent NO fragments are already present in the excited electronic state of NO_2 molecules, and a fast dissociation is assumed to occur before the statistical equilibration is reached. This model can be confirmed by the relative large averaged anisotropy parameters shown in Fig. 3(d). These β values are obtained by fitting the angular distributions of the $O(^3P_J)$ products using the following equation:

$$I(\theta) = \frac{1}{4\pi}[1 + \beta P_2(\cos\theta)] \qquad (3)$$

where θ is the angle between the recoil direction of product pairs and the polarization axis of the photolysis laser. $P_2(\cos\theta)$ is the second-order Legendre polynomial. $I(\theta)$ stands for the angular distribution. It is found that the β values change with the photolysis wavelength, and follow similar variation trends for three spin–orbit states of $O(^3P_J)$. It increases slowly from $\sim$0.4 at 365.38 nm to the maximum value of $\sim$0.8 at 300.02 nm except for a sudden increase at 357.38 nm. Generally, the variation of β values reveals that the dissociation rate of NO_2 via the 1^2B_2 state increases as the excitation wavelength decreases. Previous studies[48–50] reported that the fragmentation rate of NO_2 decreases from 50 ps close to the dissociation threshold to less than 80 fs with an excess energy of 0.1 eV above the threshold. The observed β values in the range of 0.4–0.8 correspond to a fast dissociation process, which agrees well with the averaged lifetime of $\sim$250 fs for the 1^2B_2 state estimated by Michel et al.[18]

As suggested in previous studies,[18,48–50] the 1^2B_2 state dissociation of NO_2 at different photolysis wavelengths proceeds via the nonadiabatic transition from the 1^2B_2 state to $\tilde{X}$ ground state due to a conical intersection between them, followed by a fast dissociation on this ground PESs. The photodissociation of NO_2 at all studied wavelengths in this work clearly shows non-statistical rovibrational state distributions, but the wavelength-dependent vibrational state distributions indicate that subtle differences should exist in such a dissociation pathway. Compared with the previous studies, for instance, Brouard et al.[11] reported an inverted NO vibrational state distribution at 308 nm photolysis of NO_2, which pointed to a dynamical dissociation mechanism, but their results underestimate the proportion of NO($\nu = 3$) products. While Doughty et al.[51] reported a higher yield of NO products in $\nu = 3$ at 308 nm, but were unable to extract the population in $\nu = 0$. The different experimental conditions and detection methods may be responsible for such disagreement. Nevertheless, the nascent

vibrationally hot $NO(X^2\Pi)$ product may originate from the initially populated vibrational excitation state of the NO_2 molecule. While the bimodal rotational distribution in the individual vibrational peak is consistent with bending motion caused by the geometry change on excitation mainly to the 1^2B_2 state.

B. Photodissociation of NO_2 via the 2^2B_2 state

Excitation of NO_2 in the range of 200–250 nm shows a progression of well-pronounced vibrational structures in Fig. 1, which has been assigned in terms of the quantum number $(v_1' v_2' v_3')$ of the 2^2B_2 state of the parent NO_2 molecules (v_1'-symmetric stretch, v_2'-bend, v_3'-anti-symmetric stretch). Several studies on the photodissociation of NO_2 at 212.8 nm[17,36,52] and 248 nm[18,31,33,34] were reported before. Among these previous works, only a few of them were carried out by ion imaging method.[11,35–37,53]

Fig. 4 displays the images of the $O(^3P_2)$ products and the corresponding TKER spectra transformed from the $O(^3P_2)$ images at the photolysis wavelengths of (a) 249.22 nm, (b) 246.09 nm, (c) 244.94 nm, (d) 242.36 nm, (e) 239.34 nm, (f) 237.59 nm, (g) 235.43 nm, and (h) 212.56 nm. The vibrational assignments for each TKER spectrum have been indicated in Fig. 4. Similarly, the images of the $O(^3P_1)$ and $O(^3P_0)$ products at all studied photolysis wavelengths are also presented in Fig. S3 and S4 (ESI†). It is found that the $O(^3P_J)$ images and the TKER spectra for the three $O(^3P_{J=2,1,0})$ spin–orbit dissociation channels also present similar features. But, different from those via the 1^2B_2 state, all images measured at the photolysis wavelengths in the range of 235.43–249.22 nm are characterized by a set of bright outer rings. While at 212.56 nm, the images consist of two structures, i.e., the relatively weak inner one and the strong outer one. As assigned in Fig. 4, each TKER spectrum exhibits a group of vibrational peaks extending to the available energy limit. Though Wilkinson and Whitaker[35] argued that the $NO(X^2\Pi)$ products at 226 nm favored the production of vibrationally cold, but high rotationally excited NO products, our results were consistent with that the $NO(X^2\Pi)$ products were vibrationally excited and rotationally cold. Morrell et al.[33] and Bernstein et al.[32] also attributed such sharply peaked NO to vibrationally excited, rather than rotationally excited products. At 249.22 and 246.09 nm, the major component of the TKER spectrum is a little broad compared to those at other photolysis wavelengths. While at the shortest wavelength of 212.56 nm, the TKER spectrum exhibits a pronounced bimodal structure, which is similar to that observed in the 212.8 nm photodissociation of NO_2.[36]

The vibrational state distributions of NO product for the $O(^3P_{J=2,1,0})$ channels derived by simulation of the TKER spectra are present in Fig. 5(a)–(c). It is clear that a sharply populated vibrational distribution of NO peaks at $\nu = 2$, and a tail extends to $\nu = 9$ for photolysis between 244.94 and 235.43 nm. While the major vibrational state population distribution of NO is a little broad with peaking around $\nu = 1$ at 249.22 and 246.09 nm photolysis. The low translational energy component at these two wavelengths still extends to the available energy limit. At 212.56 nm, the bimodal vibrational state distribution of NO
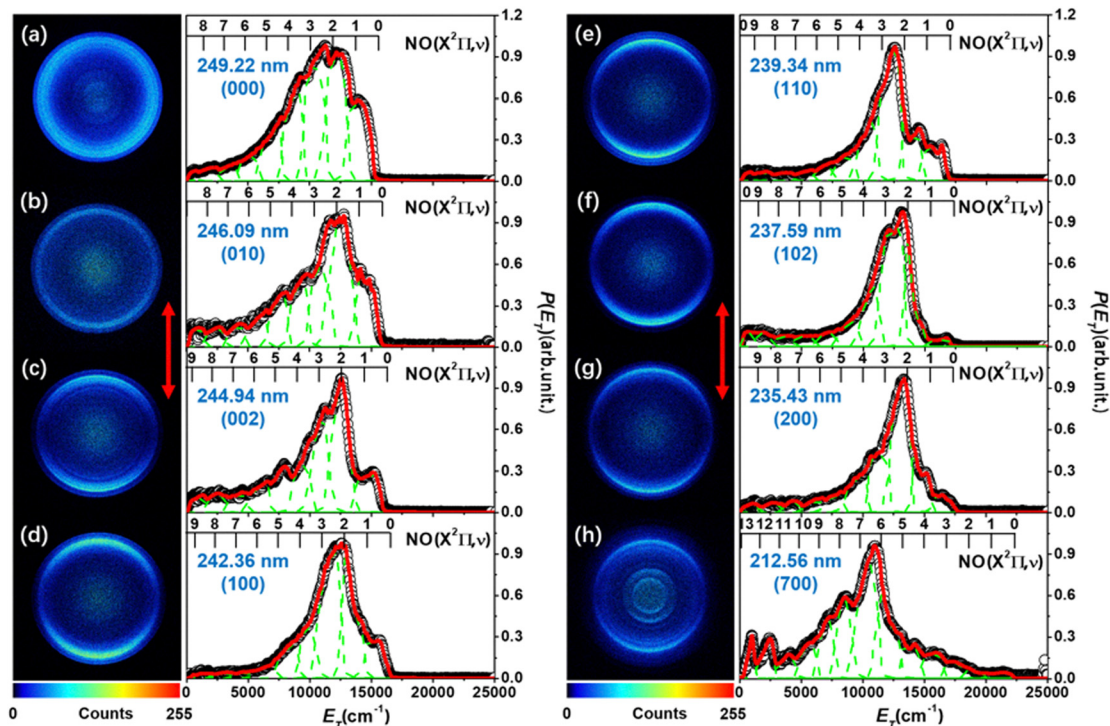
Fig. 4 The sliced images and TKER spectra of $O(^3P_2)$ products from NO_2 photodissociation at the wavelengths of (a) 249.22 nm, (b) 246.09 nm, (c) 244.94 nm, (d) 242.36 nm, (e) 239.34 nm, (f) 237.59 nm, (g) 235.43 nm, and (h) 212.56 nm. The double headed red arrow indicates the polarization direction of the photolysis laser beam. The rings shown in the images correspond to the vibrational state of the $NO(^2\Pi)$ co-products. The open circles represent the experimental data and the red solid curves display the best fitting of the experimental spectra. The dashed green curves represent the simulated NO vibrational profile.

products is more pronounced, with a major peak at $\nu = 6$ and a minor peak at $\nu = 11$, which is qualitatively consistent with that observed by Ahmed at 212.8 nm photolysis, though their results presented a major peak near $\nu = 4$.[36] Previous studies also reported that the major peak shifts to $\nu = 7$ as dissociation wavelength decreases to ~ 200 nm.[37] In addition, the rotational excitation of the NO products at studied wavelengths is found to be quite cold from the results of the TKER simulation.

To acquire more detailed information of the dissociation process *via* the 2^2B_2 state, the β values associated with the three $O(^3P_{J=2,1,0})$ spin–orbit dissociation channels are also obtained. Fig. 5(d) plots the resulting β values as a function of the photolysis wavelength for each $O(^3P_J)$ channel. Similar to those *via* the 1^2B_2 state, the β values also present a roughly similar trend for the three $O(^3P_J)$ spin–orbit dissociation channels. As shown in Fig. 5(d), the β values at 249.22 and 246.09 nm are around 0.1–0.3, indicating that the angular distributions are close to isotropic. While the β values become to range from 0.6 to 1.2 below 246.09 nm, suggesting that the angular distributions observed at short photolysis wavelengths are much anisotropic. Since different wavelengths correspond to excitation of NO_2 into different vibrational excited states of the 2^2B_2 state (marked in Fig. 4), the variation of the β values suggests that the dissociation lifetimes *via* the $2^2B_2(000)$ and $2^2B_2(010)$ vibrational states are much longer than those *via* the other vibrational states.

Previous study shows that the 2^2B_2 state PES has a shallow potential well in the Franck–Condon region and an avoided crossing with a high excited electronic state at a bond length of ~ 3.35 Å, and bond angle of $110°$.[4] At 249.22 and 246.09 nm, the initial excitation energies couldn't overcome the barrier. Thus, the excited NO_2 molecules will be trapped in the potential well of the 2^2B_2 state, resulting in a slow dissociation process and a relatively broad NO vibrational state distribution. This is consistent with previous reports on the dissociation lifetime of NO_2, *i.e.*, ~ 42 ps for the $2^2B_2(000)$ state and ~ 2.2 ps for the $2^2B_2(010)$ state.[4] While the NO_2 molecules are excited to a series of different vibrational levels of $NO_2(2^2B_2)$ between 244.94 and 212.56 nm, a direct and fast dissociation process along the symmetric stretching coordinate of the 2^2B_2 state will occur once the excitation energies exceed the barrier. During such a fast dissociation process, the nascent NO products almost inherit the internal energies of initially excited NO_2 molecules, thus the major peak in the NO vibrational state distribution shifts to a high vibrational excited level when the excitation wavelength decreases to 212.56 nm. Moreover, the interaction[11,35–38] between the 2^2B_2 state PES and the lower 1^2B_2 and/or $\tilde{X}$ state PESs *via* the vibronic coupling leads to production of kinetically cold $O(^3P_J)$ in coincidence with highly vibrationally excited NO fragments, which is associated with the minor peak close to the available energy limit. The final dissociation may happen on the $\tilde{X}$ state PES, because the 1^2B_2 state is strongly mixed with the $\tilde{X}$ state *via* a conical intersection. The bimodal energy distribution of NO products is then interpreted as NO_2 dissociation on different PESs from the initial excited 2^2B_2 state.
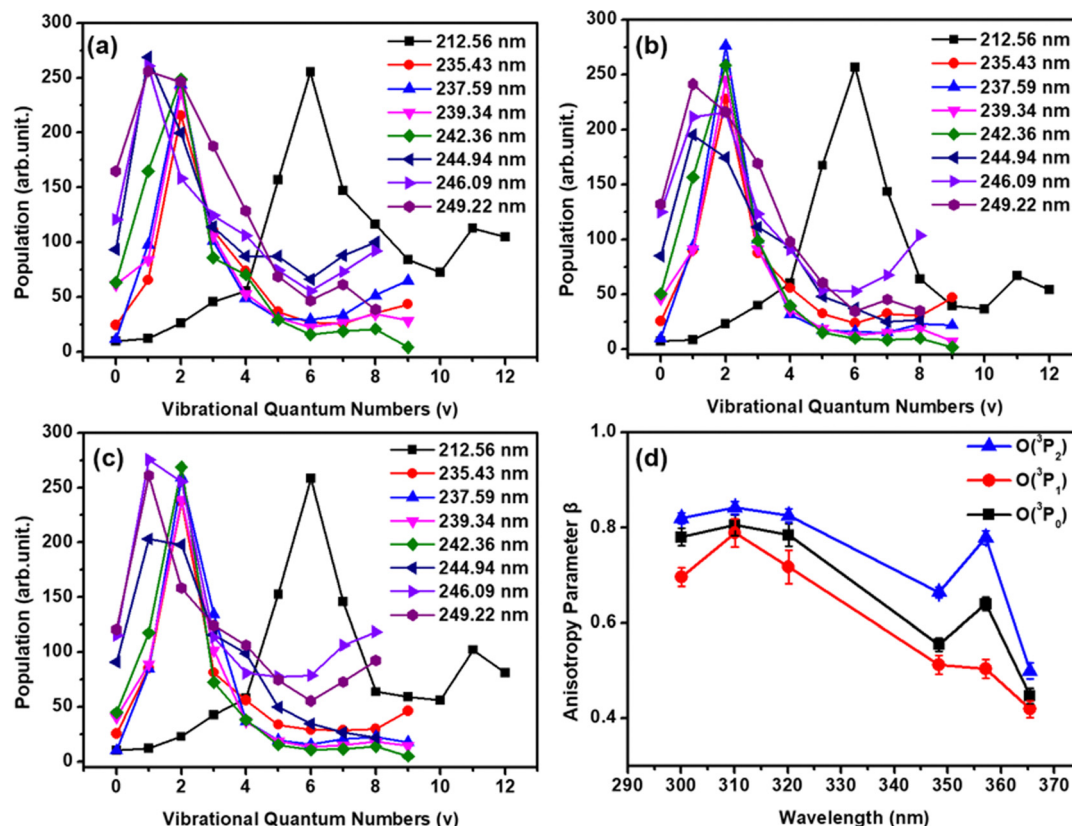
This journal is © the Owner Societies 2023

Phys. Chem. Chem. Phys., 2023, **25**, 16872–16880 | **16877**

Fig. 5 (a–c) Relative vibrational state population of the NO co-products from NO + O($^3P_{J=2,1,0}$) at eight different photolysis wavelengths between 249.22 and 212.56 nm. (d) The anisotropy parameter β values derived from simulations of the images for O($^3P_{J=2,1,0}$) products.

IV. Conclusion

In the present work, photodissociation dynamics of NO$_2$ + $h\nu \rightarrow$ NO(X$^2\Pi$) + O(^3P_j) have been investigated by using the time-sliced velocity-mapped ion imaging technique combined with the 1 + 1′ photoionization scheme. The images of O($^3P_{J=2,1,0}$) products from NO$_2$ photodissociation are acquired in the wavelength range of 300.02–365.38 nm and 212.56–249.22 nm, which correspond to excitation of the 1$^2B_2$ and 2$^2B_2$ states, respectively. The TKER spectra and NO vibrational state distributions are derived based on the images of O($^3P_{J=2,1,0}$) products. The non-statistical vibrational state distribution of NO and the bimodal rotational structure in most of the vibrational peak have been observed between 365.38 and 300.02 nm. This result indicates that the high bending vibrational excitation due to the change in NO$_2$ geometry following decay from the 1$^2B_2$ state to the X̃ state leads to hot rotational excitation of NO. While the NO vibrational state distribution from NO$_2$ photodissociation *via* a series of vibrational levels of the 2$^2B_2$ state is sharply peaked at low vibrational quantum number v, and this vibrational peak shifts to larger v as the excitation energy increases. A bimodal vibrational population distribution has been observed at 212.56 nm, which is ascribed to NO$_2$ dissociation on two different pathways. Furthermore, the anisotropy parameter β values associated with dissociation *via* the two $^2B_2$ states display wavelength-dependent characters. The overall β value from excitation of the 1$^2B_2$ state shows an increasing tendency as the photolysis wavelength decreases except at 357.13 nm, suggesting the dissociation

occurs *via* a fast transition from the 1$^2B_2$ state to the X̃ state *via* a conical intersection between them. While the β values from excitation of the 2$^2B_2$ state at short wavelength suggest that the dissociation on the 2$^2B_2$ state PES is fast *via* an avoided crossing with the higher state PES, except the relatively slow dissociation at 249 nm and 246 nm due to the energies being lower than the barrier of the 2$^2B_2$ state PES. In addition, the interaction between the 2$^2B_2$ state and the lower 1$^2B_2$ and/or X̃ state *via* the vibronic coupling leads to the minor peak at a very high vibrational level at 212.56 nm photolysis. Though we have presented a detailed state-resolved photodissociation of NO$_2$, a full understanding of the dissociation mechanism still awaits further theoretical calculations.

Author contributions

Shengrui Yu and Kaijun Yuan designed the experiments. Zhaoxue Zhang, Shuaikang Yang, Zhenxing Li, Yao Chang, Zijie Luo and Yarui Zhao performed the experiments. Zhaoxue Zhang, Zhenxing Li and Yao Chang analyzed the data. Shengrui Yu, kaijun Yuan and Xueming Yang discussed the data, Shengrui Yu, Zhenxing Li and kaijun Yuan prepared the manuscript. All the authors edited, discussed and approved the whole paper.

Conflicts of interest

The authors declare no competing interests.

Acknowledgements

References

1 H. Katagiri and S. Kato, *J. Chem. Phys.*, 1993, **99**, 880–8815.

2 R. Schinke, S. Y. Grebenshchikov and H. Zhu, *Chem. Phys.*, 2008, **346**, 99–114.

3 M. F. Mrienne, A. Jenouvrier and B. Coquart, *J. Atmos. Chem.*, 1995, **20**, 281–297.

4 S. Li, J. Matthews and A. Sinha, *Science*, 2008, **319**, 1657–1660.

5 B. Coquart, A. Jenouvrier and M. F. Merienne, *J. Atmos. Chem.*, 1995, **21**, 251–261.

6 A. Jenouvrier, B. Coquart and M. F. Merienne, *J. Atmos. Chem.*, 1996, **25**, 21–32.

7 W. Schneider, G. K. Moortgat, G. S. Tyndall and J. P. Burrows, *J. Photoch. Photobio. A*, 1987, **40**, 195–217.

8 I. Wilkinson, I. A. Garcia, B. J. Whitaker, J. B. Hamard and V. Blanchet, *Phys. Chem. Chem. Phys.*, 2010, **12**, 15766–15779.

9 G. E. Busch and K. R. Wilson, *J. Chem. Phys.*, 1972, **56**, 3638–3654.

10 R. Jost, J. Nygård, A. Pasinski and A. Delon, *J. Chem. Phys.*, 1996, **105**, 1287–1290.

11 M. Brouard, R. Cireasa, A. P. Clark, T. J. Preston and C. Vallance, *J. Chem. Phys.*, 2006, **124**, 64309.

12 Y. Mo, H. Katayanagi and T. Suzuki, *J. Chem. Phys.*, 1999, **110**, 2029–2041.

13 C. H. Hsieh, Y. S. Lee, A. Fujii, S. H. Lee and K. Liu, *Chem. Phys. Lett.*, 1997, **277**, 33–38.

14 J. A. Harrison, X. Yang, M. Roesslein, P. Felder and J. R. Huber, *J. Phys. Chem.*, 1994, **98**, 12260–12269.

15 C. Ning, H. Lin and J. Pfab, *J. Phys. Chem.*, 1993, **97**, 7458–7464.

16 V. P. Hradil, T. Suzuki, S. A. Hewitt, P. L. Houston and B. J. Whitaker, *J. Chem. Phys.*, 1993, **99**, 4455–4463.

17 J. Miyawaki, T. Tsuchizawa, K. Yamanouchi and S. Tsuchiya, *Chem. Phys. Lett.*, 1990, **165**, 168–170.

18 M. Mons and I. Dimicoli, *Chem. Phys.*, 1989, **130**, 307–324.

19 P. A. Elofson and E. Ljungström, *Chem. Phys.*, 1992, **165**, 323–337.

20 K. Chen and C. Pei, *Chem. Phys. Lett.*, 1987, **137**, 361–364.

21 H. Zacharias, M. Geilhaupt, K. Meier and K. H. Welge, *J. Chem. Phys.*, 1981, **74**, 218–225.

22 J. Miyawaki, T. Tsuchizawa, K. Yamanouchi and S. Tsuchiya, *Chem. Phys. Lett.*, 1990, **165**, 168–170.

23 G. Hancock, P. J. Pearson, G. A. D. Ritchie and D. F. Tibbetts, *Phys. Chem. Chem. Phys.*, 2003, **5**, 5386–5391.

24 M. Brouard, P. O'Keeffe, D. M. Joseph and D. Minayev, *Phys. Rev. Lett.*, 2001, **86**, 2249–2252.

25 K. E. J. Hallin and A. J. Merer, *Can. J. Phys.*, 1976, **54**, 1157–1171.

26 K. Tsuji, M. Ikeda, J. Awamura, A. Kawai and K. Shibuya, *Chem. Phys. Lett.*, 2003, **374**, 601–607.

27 R. Fan and L. D. Ziegler, *J. Raman Spectrosc.*, 1994, **25**, 497–506.

28 W. M. Uselman and E. K. C. Lee, *J. Chem. Phys.*, 1976, **65**, 1948–1955.

29 F. Sun, G. P. Glass and R. F. Curl, *Chem. Phys. Lett.*, 2001, **337**, 72–78.

30 G. Hancock and M. Morrison, *Mol. Phys.*, 2005, **103**, 1727–1733.

31 T. G. Slanger, W. K. Bischel and M. J. Dyer, *J. Chem. Phys.*, 1983, **79**, 2231–2240.

32 H. S. Im and E. R. Bernstein, *J. Phys. Chem. A*, 2002, **106**, 7565–7572.

33 C. B. Claire Morrell, Vanessa Haverd, Aimee Cawley and Gus Hancock, *J. Chem. Phys.*, 2002, **117**, 11121–11130.

34 J. McFarlane, J. C. Polanyi and J. G. Shapter, *J. Photochem. Photobiol. A*, 1991, **58**, 139–172.

35 I. Wilkinson and B. J. Whitaker, *J. Chem. Phys.*, 2008, **129**, 154312.

36 M. Ahmed, D. S. Peterka, A. S. Bracker, O. S. Vasyutinskii and A. G. Suits, *J. Chem. Phys.*, 1999, **110**, 4115–4118.

37 A. M. Coroiu, D. H. Parker, G. C. Groenenboom, J. Barr, I. T. Novalbos and B. J. Whitaker, *Eur. Phys. J. D*, 2006, **38**, 151–162.

38 I. Wilkinson, M. P. de Miranda and B. J. Whitaker, *J. Chem. Phys.*, 2009, **131**, 054308.

39 Z. Li, M. Zhao, T. Xie, Y. Chang, Z. Luo, Z. Chen, X. Wang, K. Yuan and X. Yang, *Mol. Phys.*, 2020, **119**, e1813911.

40 J. Zhou, Y. Zhao, C. S. Hansen, J. Yang, Y. Chang, Y. Yu, G. Cheng, Z. Chen, Z. He, S. Yu, H. Ding, W. Zhang, G. Wu, D. Dai, C. M. Western, M. N. R. Ashfold, K. Yuan and X. Yang, *Nat. Commun.*, 2020, **11**, 1547.

41 Z. Li, M. Zhao, T. Xie, Z. Luo, Y. Chang, G. Cheng, J. Yang, Z. Chen, W. Zhang, G. Wu, X. Wang, K. Yuan and X. Yang, *J. Phys. Chem. Lett.*, 2021, **12**, 844–849.

42 Y. Zhao, Z. Luo, Y. Chang, Y. Wu, S. Zhang, Z. Li, H. Ding, G. Wu, J. S. Campbell, C. S. Hansen, S. W. Crane, C. M. Western, M. N. R. Ashfold, K. Yuan and X. Yang, *Nat. Commun.*, 2021, **12**, 4459.

43 C. Ling, H. Liao, D. Yuan, W. Chen, Y. Tan, W. Li, S. Yu, X. Yang and X. Wang, *Phys. Chem. Chem. Phys.*, 2021, **23**, 5809–5816.

44 M. Zhao, Z. Li, T. Xie, Y. Chang, F. Wu, Q. Wang, W. Chen, T. Wang, X. Wang, K. Yuan and X. Yang, *Chin. J. Chem. Phys.*, 2021, **34**, 95–101.

This journal is © the Owner Societies 2023

Phys. Chem. Chem. Phys., 2023, **25**, 16872–16880 | **16879**

45 C. G. Stevens and R. N. Zare, *J. Mol. Spectrosc.*, 1975, **56**, 167–187.

46 G. D. Gillispie, A. U. Khan, A. C. Wahl, R. P. Hosteny and M. Krauss, *J. Chem. Phys.*, 1975, **63**, 3425–3444.

47 G. E. Busch and K. R. Wilson, *J. Chem. Phys.*, 1972, **56**, 3626–3638.

48 S. I. Ionov, G. A. Brucker, C. Jaques, Y. Chen and C. Wittig, *J. Chem. Phys.*, 1993, **99**, 3420–3435.

49 I. Bezel, P. Ionov and C. Wittig, *J. Chem. Phys.*, 1999, **111**, 9267–9279.

50 I. Bezel, D. Stolyarov and C. Wittig, *J. Phys. Chem. A*, 1999, **103**, 10268–10273.

51 A. Doughty, G. Hancock and E. L. Moore, *Chem. Phys. Lett.*, 1997, **274**, 58–62.

52 R. C. Richter, V. I. Khamaganov and A. J. Hynes, *Chem. Phys. Lett.*, 2000, **319**, 341–348.

53 M. Ahmed, D. S. Peterka and A. G. Suits, 21st International Symposium on Rarefied Gas Dynamics, Marseille, France, July 26–31, 1998.